AFRL-RH-WP-TR-2014-0107

PLASMONIC APTAMER-GOLD NANOPARTICLE SENSORS FOR SMALL MOLECULE FINGERPRINT IDENTIFICATION

Jorge Chávez
Grant Slusher
UES Inc.
4401 Dayton-Xenia Road
Dayton, OH 45432

Joshua Hagen
Nancy Kelley-Loughnane
Human Signatures Branch

Juliann Leny
Suzanne Witt
Wright Scholar Program

AUGUST 2014
Interim Report

AIR FORCE RESEARCH LABORATORY
711TH HUMAN PERFORMANCE WING,
HUMAN EFFECTIVENESS DIRECTORATE,
WRIGHT-PATTERSON AIR FORCE BASE, OH 45433
AIR FORCE MATERIEL COMMAND
UNITED STATES AIR FORCE

STINFO COPY

NOTICE AND SIGNATURE PAGE

Using Government drawings, specifications, or other data included in this document for any purpose other than Government procurement does not in any way obligate the U.S. Government. The fact that the Government formulated or supplied the drawings, specifications, or other data does not license the holder or any other person or corporation; or convey any rights or permission to manufacture, use, or sell any patented invention that may relate to them.

This report was cleared for public release by the 88th Air Base Wing Public Affairs Office and is available to the general public, including foreign nationals. Copies may be obtained from the Defense Technical Information Center (DTIC) (http://www.dtic.mil).

AFRL-RH-WP-TR-2014-0107 HAS BEEN REVIEWED AND IS APPROVED FOR PUBLICATION IN ACCORDANCE WITH ASSIGNED DISTRIBUTION STATEMENT.

//signature//

NANCY KELLEY-LOUGHNANE, Ph.D.
Work Unit Monitor
Human Signatures Branch

//signature//

LOUISE CARTER, Ph.D.
Chief, Human-Centered ISR Division
Human Effectiveness Directorate
711th Human Performance Wing
Air Force Research Laboratory

This report is published in the interest of scientific and technical information exchange, and its publication does not constitute the Government's approval or disapproval of its ideas or findings.

REPORT DOCUMENTATION PAGE

Form Approved
OMB No. 0704-0188

1. REPORT DATE *(DD-MM-YY)*	2. REPORT TYPE	3. DATES COVERED *(From - To)*
20 08 14	Interim	1 October 2011 – 30 April 2014

4. TITLE AND SUBTITLE
Plasmonic Aptamer-Gold Nanoparticle Sensors for Small Molecule Fingerprint Identification

5a. CONTRACT NUMBER
N/A

5b. GRANT NUMBER

5c. PROGRAM ELEMENT NUMBER

6. AUTHOR(S)
Jorge L Chávez
Grant M. Slusher
Joshua A. Hagen
Nancy Kelley-Loughnane[a]
Juliann Leny
Suzanne Witt

5d. PROJECT NUMBER

5e. TASK NUMBER

5f. WORK UNIT NUMBER
H05B (7184D417)

7. PERFORMING ORGANIZATION NAME(S) AND ADDRESS(ES)
UES Inc.
4401 Dayton-Xenia Road
Dayton, OH 45432

8. PERFORMING ORGANIZATION REPORT NUMBER

9. SPONSORING/MONITORING AGENCY NAME(S) AND ADDRESS(ES)
Air Force Materiel Command
Air Force Research Laboratory
711th Human Performance Wing
Human Effectiveness Directorate
Human-Centered ISR Division
Human Signatures Branch
Wright-Patterson AFB, OH 45433

10. SPONSORING/MONITORING AGENCY ACRONYM(S)
711 HPW/RHXB

11. SPONSORING/MONITORING AGENCY REPORT NUMBER(S)
AFRL-RH-WP-TR-2014-0107

12. DISTRIBUTION/AVAILABILITY STATEMENT
Distribution A: Approved for public release; distribution is unlimited.

13. SUPPLEMENTARY NOTES
88ABW-2014-4109, Cleared 29 August 14

14. ABSTRACT The utilization of the plasmonic response of aptamer -gold nanoparticle conjugates (Apt-AuNPs) to design cross-reactive arrays for fingerprint identification of small molecular targets was demonstrated for the first time. Four aptamers with different structural features previously selected to bind different targets were used in combination with AuNPs by adsorbing the DNA on the AuNPs surface. The optimized response of the Apt-AuNPs to the analytes showed that, depending on the specific aptamer used, target binding by the aptamer could result in an increase or decrease of Apt-AuNPs stability. These Apt-AuNPs showed the ability to recognize different analytes with different affinities, generating fingerprints that allowed unambiguous analyte identification with response times in less than fifteen minutes. Importantly, it was observed that it was not necessary to select an aptamer per analyte of interest to generate differentiable signatures, but a subset of aptamers could be use to identify a larger number of analytes. The data was analyzed using principal component analysis, showing efficient clustering of the different datasets for qualitative and quantitative identification. This work opens the door to using these Apt-AuNPs in point of care diagnostics applications where fast sensors with easy to read outputs are needed.

15. SUBJECT TERMS
Plasmonic, aptamer-gold nanoparticle conjugates

16. SECURITY CLASSIFICATION OF:			17. LIMITATION OF ABSTRACT:	18. NUMBER OF PAGES	19a. NAME OF RESPONSIBLE PERSON (Monitor)
a. REPORT	b. ABSTRACT	c. THIS PAGE			Nancy Kelley-Loughnane, Ph.D.
U	U	U	SAR	26	19b. TELEPHONE NUMBER *(Include Area Code)* N/A

Standard Form 298 (Rev. 8-98)
Prescribed by ANSI Std. Z39-18

THIS PAGE LEFT BLANK INTENTIONALLY.

TABLE OF CONTENTS

Plasmonic Aptamer-Gold Nanoparticle Sensors for Small Molecule Fingerprint Identification

Jorge L Chávez[a], Juliann Leny[a,b], Suzanne Witt[b,c], Grant M. Slusher[a], Joshua A. Hagen[a] and Nancy Kelley-Loughnane[*aXXXXX]

Received (in XXX, XXX) Xth XXXXXXXXX 20XX, Accepted Xth XXXXXXXXX 20XX
DOI: 10.1039/b000000x

The utilization of the plasmonic response of aptamer-gold nanoparticle conjugates (Apt-AuNPs) to design cross-reactive arrays for fingerprint identification of small molecular targets was demonstrated for the first time. Four aptamers with different structural features previously selected to bind different targets were used in combination with AuNPs by adsorbing the DNA on the AuNPs surface. The optimized response of the Apt-AuNPs to the analytes showed that, depending on the specific aptamer used, target binding by the aptamer could result in an increase or decrease of Apt-AuNPs stability. These Apt-AuNPs showed the ability to recognize different analytes with different affinities, generating fingerprints that allowed unambiguous analyte identification with response times in less than fifteen minutes. Importantly, it was observed that it was not necessary to select an aptamer per analyte of interest to generate differentiable signatures, but a subset of aptamers could be use to identify a larger number of analytes. The data was analyzed using principal component analysis, showing efficient clustering of the different datasets for qualitative and quantitative identification. This work opens the door to using these Apt-AuNPs in point of care diagnostics applications where fast sensors with easy to read outputs are needed.

Introduction

The design of sensors that detect different metabolites simultaneously with fast responses would improve the field of medical diagnostics and facilitate the development of personalized medicine[1]. Biomarker monitoring involves not only the detection of specific targets, but more importantly, changes in their concentrations that could be indicative of specific health conditions.[2,3] Most of the efforts in sensor design are focused on systems that detect one target at the time with great selectivity and specificity[4,5]. However, when the goal is to characterize a disease or the health status of an individual, monitoring the levels of multiple biomarkers simultaneously would provide a more complete characterization and potentially would result in better prognosis[6,7].

Applications requiring simultaneous monitoring of different targets might benefit from sensors that interact with multiple analytes with different specificities[8]. In these multiplex systems, like the human nose and tongue, the identification of one compound is realized by the analysis of a target fingerprint with an array of sensors with cross-reactive responses to different analytes[9,10]. Importantly, this sensing approach is less prone to result in false positives since the detection of a particular target is based on the response of multiple sensing units to the same target. When only one of the sensing elements failed resulting in false identification of an analyte, the error is easily noticed by the lack of response of the other sensing elements to this analyte, since the probability of having all sensors failing simultaneously is very low[11].

Aptamers have shown great promise as biorecognition elements for biosensors providing great sensitivity and selectivity for a wide range of analytes[12,13,14]. The ease of their chemical modification and their chemical and thermal stability made them valuable capture elements for sensor design[15]. It has been demonstrated that the sequence of certain aptamer clones can be optimized to tune their selectivity from one target to a family of chemically related analytes. For instance, different clones of a cholic acid-binding aptamer were studied and a response to multiple hydrophobic steroids was observed by some of these clones[16]. Similarly, the well-known cocaine binding aptamer was mutated in specific positions close to the binding site to promote binding to a series of steroids and create cross-reactive arrays[17]. In a different approach, SELEX has been modified by alternating the target a random pool of RNA was exposed to, achieving aptamer sequences that recognized the chemical core of a family of related compounds[18]. These examples show that the binding properties of aptamers could be advantageous to design cross-reactive arrays for simultaneous multiplex analyte detection[19].

Gold nanoparticles (AuNPs) have been used in a number of sensing approaches due to their colorimetric response to events that affect their stability[20,21]. Aptamers have been utilized with AuNPs to create fast colorimetric sensors for different targets, ranging from ions[22] to small molecules[23,24,25] and proteins[26]. The typical colorimetric assay with aptamers and AuNPs is based on the difference in affinity of AuNPs for single stranded DNA (*ss*-DNA) and double stranded DNA (*ds*-DNA). It has been demonstrated that *ss*-DNA adsorbed fast on the AuNPs surface, while AuNPs showed a much poorer affinity for *ds*-DNA[27]. In general, it has been proposed that target binding by an aptamer occurs with a conformational switch from a *ss*-DNA-like conformation in the absence of the target to a *ds*-DNA-like conformation after target binding[28]. Therefore, an aptamer exposed to a non-target analyte remained as *ss*-DNA and adsorbed on the AuNPs improving their stability due to the addition of negative charges to the AuNPs surface. On the contrary, an aptamer bound to its target, with a *ds*-DNA-like conformation, did not adsorb on the AuNPs and provided no improvement in stability. Experimentally, to detect a target with these sensors, an aptamer is exposed to the sample of interest and, after a short incubation time, AuNPs are added to the mixture.

After the AuNPs and aptamer are allowed to interact, salt is added to test the stability of the AuNPs. The presence of the target and the formation of the *ds*-like DNA conformation after binding resulted in AuNPs aggregation with a color change to blue after salt addition (no DNA adsorption on AuNPs, no increase in stability). On the other hand, in the absence of the target, the AuNPs suspensions remained red (free aptamer adsorbed on the AuNPs, increased stability). We have observed when using this detection scheme, that a non-target analyte that remains free in solution after aptamer addition can potentially interact with the AuNPs surface affecting their stability, which resulted in false positives[29]. To prevent the non-specific interactions between unbound target and the AuNPs surface, the colorimetric assays used here involved aptamer adsorption on the AuNPs prior to target addition. These aptamer-AuNPs conjugates (Apt-AuNPs) were prepared by simply mixing the two components followed by buffer addition and an overnight incubation. The presence of the DNA prevented non specific interactions, while allowing a colorimetric response to the aptamer target, as reported previously by our group[29].

In the last few years, nanomaterials have been interfaced with bio-recognition elements (BREs) to design cross-reactive sensors for multiplex protein detection. The Rotello group has demonstrated nanoparticle-based cross-reactive sensing for identification of different types of proteins and cells with a fluorescence output[8, 30,31], and recently the plasmonic response of aptamer-modified nanorods to binding events was used for multiplexed protein detection[19]. Very recently, the use of the label-free plasmonic response of Apt-AuNPs in cross-reactive sensors for protein targets has been demonstrated[32,19]. Small molecular targets non-plasmonic multiplex detection based on aptamers has been recently demonstrated using fluorescence detection[33] and SERS[34]. However, the multiplex plasmonic identification of small molecular analytes has not been demonstrated to the best of our knowledge. Small molecules are challenging targets for cross-reactive sensors since they have lower number of functional groups compared to proteins, which makes their classification difficult. In this work, we designed a library of Apt-AuNPs with four aptamers: adenosine binding aptamer (ABA)[35], riboflavin-binding aptamer (RBA)[36], estradiol-binding aptamer (EBA)[37] and cholic acid-binding aptamer (CABA)[38]. The colorimetric response of these Apt-AuNPs to their targets and the other analytes in this set was fully characterized. Importantly, while performing these studies an exciting phenomenon was observed: the effect of aptamer binding to its target on AuNPs stability depended on the aptamer used, and could result in an increase or decrease of particle stability. The aptamers used in this sensing scheme showed the ability to respond to multiple targets with different affinities. We demonstrated in this work that different fingerprints were obtained based on the combined response of the Apt-AuNPs to each of the analytes studied. Moreover, principal components analysis (PCA) was used to efficiently cluster the data, demonstrating that this library of Apt-AuNPs show great potential to be used as a cross-reactive arrays for multiplex detection of chemically similar molecules.

Experimental Section

Materials

Riboflavin, 17-β-estradiol, hydrogen tetrachloroaurate(III) ($HAuCl_4$), sodium citrate, sodium chloride (NaCl) , magnesium chloride ($MgCl_2$), cholic acid, adenosine, tris-HCl and potassium chloride (KCl) were obtained from Sigma-Aldrich (St. Louis, MO). HEPES buffer was purchased from Amresco Inc. (Solon, OH) All chemicals were of analytical grade and used without further purification.

DNA Synthesis

All synthesis reagents were purchased from Glen Research (Sterling VA 20164), except where noted. All oligonucleotides were synthesized in-house using the following protocol: The phosphoramidite method of oligonucleotide synthesis was performed on an ABI 394 eight column DNA/RNA Synthesizer. Sequences were grown from a 3' end solid support base followed by a standard progression of 1) oxidation (washing with 0.02M I_2 in THF/Pyridine/H_2O); 2) detritylation (washing with 3% TCA/DCM) 3) coupling (introducing appropriate T,A,C, or G phosphoramadite) 4) capping (THF/Pyridine/Ac_2O) and 5) a final oxidation step to remove trace H_2O from the reaction chamber. For de-protection and purification, the glass beads attached to the base of the newly formed DNA were transferred to the bottom of a 25 mL glass test tube. Then 3 mL of a 1:1 Ammonium Hydroxide:Methylamine (Sigma-Aldrich St. Louis MO) solution was added to the tube. The tube and its contents were incubated at 65 °C for 30 min. After removal from the incubator 250 µL of 3M NaCl was pipetted into the mixture and vortexed briefly. Ice cold ethanol was added in 6 mL aliquot and the mixture was placed in the freezer for 30 min. After the sample test tube was removed the mixture was applied to a NAP-5 desalting column (GE Healthcare Bio-Sciences Pittsburgh, PA 15264) in 1 mL fractions. Fractions were collected in 1.5 mL micro centrifuge tubes and concentrated using an Eppendorf Vacufuge (Eppendorf Hauppauge, NY 11788). Samples were then re-suspended to working concentrations using DNAse free H_2O.

AuNPs Synthesis and Characterization

The AuNPs were synthesized as reported previously[24]. In brief, 98 mL of deionized water (Millipore, Billerica,MA) were mixed with 2 mL of 50 mM $HAuCl_4$, heated and refluxed. As soon as reflux started, 10 mL of a 38.8 mM sodium citrate solution was added. The solution turned red after a few minutes. Heat was discontinued and the reaction was allowed to continue for 20 min under constant stirring. Subsequently, the suspension was allowed to cool down and filtered with a 0.2 µm polyester membrane. The AuNPs suspensions were kept in the dark when not in use at RT. The AuNPs size was determined to be 15 nm by dynamic light scattering (DLS). The extinction maximum was determined to be 520 nm in a Cary 300 UV spectrophotometer (Agilent Technologies, Santa Clara, CA). The AuNP concentration was calculated to be 10 nM, based on a molar absorption coefficient of 2.4×10^8 L mol^{-1} cm^{-1}.

Assay Design

AuNP-aptamer conjugates (80 aptamers per AuNP) were prepared by mixing 2 mL 10 nM AuNPs (15 nm) with 16 µL of 100 µM DNA. These mixtures were allowed to incubate for at least 2 hours and then were diluted 1:1 with 10 mM HEPES, 1 mM $MgCl_2$ buffer. This mixture was then left to incubate overnight. The Apt-AuNPs were typically used within three days after their preparation. In the case of the ABA- and EBA-AuNPs, the first step in the assay optimization was to determine the NaCl needed to promote a mild aggregation of the AuNPs exposed to a blank sample. Once the NaCl concentration was set, the same experiment was performed with a sample containing the aptamer's target (adenosine for ABA and estradiol for EBA). A higher aggregation response was observed in the presence of the target in each case. The NaCl concentration was adjusted again to maximize the difference in response between the blank and the target-containing samples. Finally, the linear range of the response was determined and each analyte was tested in this concentration range with the other Apt-AuNPs. In the case of the CABA and RBA, the Apt-AuNPs were exposed to NaCl concentration that promoted severe aggregation, since preliminary data showed that target binding increased the Apt-AuNPs stability. Once the optimal NaCl concentration to promote Apt-AuNPs aggregation in the presence of a blank was determined, similar experiments were performed in the presence of the target, followed by assay optimization.

Analyte Detection

To prepare the targets, a 100 mM stock solution of adenosine, estradiol, and cholic acid and a 10 mM stock solution of riboflavin were made by dissolving the analytes in dimethyl sulfoxide. Then each target was diluted down with the appropriate buffer to the concentrations reported in the plots. Estradiol and adenosine were diluted using a 1/3 Strength Estradiol Binding Buffer (33.3 mM Tris-HCl, 66.7 mM NaCl, 8.3 mM KCl, 3.3 mM $MgCl_2$, 1.7% EtOH). Riboflavin and cholic acid were diluted using the 10 mM HEPES, 1 mM $MgCl_2$ buffer. AuNPs (75 µL) were mixed with 10 µL of the analyte stock solution. The mixtures were incubated for 10 min in a 96-well plate, protected from light. Subsequently, a volume of a 2 M NaCl solution was added simultaneously to all the wells used in an experiment to obtain the same final salt concentration. After briefly mixing the samples, the plate was immediately transferred to a Spectra Max M5 plate reader (Molecular Devices, Sunnyvale, CA) and the extinction of the AuNP suspensions at 530 and 650 nm was recorded. The degree of aggregation was plotted as the ratio of the extinction intensity of the aggregated AuNPs (extinction at 650 nm) over the individual AuNPs (extinction at 530 nm) as a function of target concentration.

Principal Component Analysis

For PCA analysis, five replicates of the response of each Apt-AuNP to each analyte at a concentration of 15 and 20 µM were obtained. The data was analyzed with XLSTAT software.

Results and Discussion

Apt-AuNP Library Design

Four aptamers reported in the literature were selected to design Apt-AuNPs by the following criteria (see Table 1 for sequences): they bind to small molecules with relatively similar structures (see Figure 1A for chemical structures), they have different lengths, and their predicted secondary structures are significantly different (See Figure 1B for a schematic representation of their conformations and Figure S1 for mfold predicted structures). The use of aptamers with different structural features was intended to increase the probability of having different interactions between each analyte and the different aptamers, increasing the chances of obtaining different fingerprints. Using analytes with relatively similar structures but that do not belong to the same family, was expected to provide a means to study the cross-reactivity of these Apt-AuNPs. It is important to consider that the selectivity and affinity of the aptamer free in solution could be affected by aptamer immobilization on a surface. In the case studied here, the aptamers are adsorbed on the AuNPs surface, interacting strongly with the AuNPs through the interaction of multiple nucleotides, which could alter target binding thermodynamics and kinetics.

Table 1 Sequences of the Aptamers used in this Study

Name	Sequence
ABA	ACCTGGGGGAGTATTGCGGAGGAAGGT
EBA	GCTTCCAGCTAATTGAATTACACGCAGAGGGTAGCGGCTCTG CGCATTCAATTGCTGCGCGCTGAAGCGCGGAAGC
CABA	GCAGGGTCAATGGAATTAATGATCAATTGACAGACGCAAGTC TCCTGC
RBA	TTTTTTTTTTGGAACGACGGTGGTGGAGGAGATCGTTCC

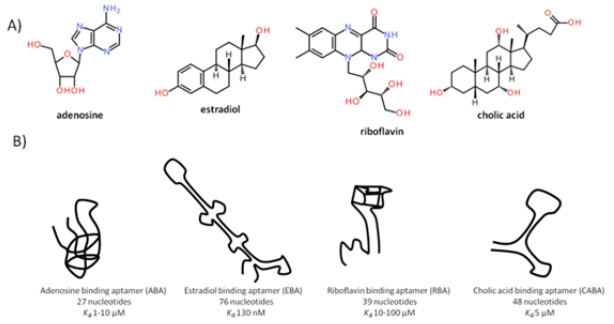

Fig. 1 A) Chemical structures of analytes used in this study, B): Schematic representation of the experimentally reported structures of the aptamers used here, (see Figure S1 for mfold predicted structures).

Effect of Analyte Adsorption on Citrate-Stabilized AuNPs Stability

It is well-known that different species with amine and hydroxyl groups, especially proteins, interact strongly with the surface of citrate-stabilized AuNPs[39,40]. Their adsorption on AuNPs can result in an increase or decrease in the AuNPs tendency to aggregate in media with high ionic strength, depending on the functional groups and structure of each protein. Figure S2 shows that the small molecule analytes used here interacted strongly with the AuNPs, as well. The plot shows the citrate-stabilized AuNP degree of aggregation: the ratio of AuNPs extinction at

650 nm (blue, aggregated AuNPs) and 530 nm (red, well-dispersed AuNPs), in the presence of each analyte (180 µM) before and after salt addition. It was observed that addition of adenosine, estradiol and riboflavin resulted in AuNPs aggregation when NaCl was added, while cholic acid resulted in AuNPs stabilization against salt-induced aggregation. Due to this, it was decided that to help prevent non-specific interactions between the analytes and the AuNPs, the DNA aptamers were going to be deposited on the AuNPs surface *before* analyte detection, as discuss next.

Colorimetric Sensing with Apt-AuNPs

The aptamer was allowed to adsorb on the AuNPs by an overnight incubation to prevent non-specific interactions between the surface-active analytes and AuNPs, as we have demonstrated previously[29]. The resulting Apt-AuNPs showed improved stability against salt-induced aggregation compared to the AuNPs non-exposed to the DNA, as observed by the higher NaCl concentration needed to obtain a change in color from red to blue. Importantly, the amount of NaCl needed to promote the Apt-AuNPs aggregation was different for each aptamer, despite the fact that all aptamers were loaded at the same density: 80 aptamer/AuNP and they were all suspended in the same buffer. This was interpreted as evidence that each aptamer interacted differently with the AuNPs, probably due to a combination of the different aptamer lengths and structures. The first step in this work was to characterize the response of each Apt-AuNP to the four analytes studied here. In the first step, an aptamer was chosen to prepare Apt-AuNPs and the conjugates were exposed to the aptamer's target to determine the dynamic range of the response. The NaCl concentration needed to promote Apt-AuNPs aggregation was optimized independently for each Apt-AuNPs. In the second step, the same analyte was used to test the other Apt-AuNPs in the analyte concentration range determined in the first step. This protocol was repeated consistently for each Apt-AuNP-target sets. Each data set in a graph is normalized to the value of the blank for ease of comparison. Importantly, in all cases, the response of these Apt-AuNPs was obtained after ten minute incubation with the target followed by two minute incubation with salt, showing promise to develop fast colorimetric sensors. The variance of the data is shown in the graphs as the standard deviation of three replicates.

The response obtained with Apt-AuNPs made with the adenosine-binding aptamer (ABA-AuNPs) is shown in Figure 2A and B. The ABA is a short sequence that has been shown to form an extended pseudohelix in the binding complex that accommodates two adenosine molecules[41]. The ABA-AuNPs showed the typical response for this type of colorimetric assays, a large aggregation response in the presence of adenosine with minimal response to non-target analytes. This confirms that the DNA adsorption on the AuNPs surface prevented non-specific interactions between the AuNPs and the other analytes. Figure S3 shows TEM images of the ABA-ANPs exposed to buffer (Figure S3A) and adenosine (Figure S3B) after NaCl addition, confirming that the colorimetric response observed was due to AuNPs aggregation triggered by the target binding. The Apt-AuNPs designed with the estradiol binding aptamer (EBA-AuNPs) on the other hand, showed a large response to estradiol and riboflavin, a milder response to adenosine and no response to cholic acid, as shown in Figure 2C and D. The reason for this lack of selectivity is not clear yet. The EBA is the longest aptamer used here, with long stretches of paired nucleotides and four small loops[37], as shown schematically in Figure 1A (see Figure S1, for mfold prediction). We hypothesized that this lack of selectivity could be due to: i) interactions between the aptamer and the AuNPs surface that affected the aptamer conformation, and/or ii) the lack of strong interactions between the paired nucleotides and the AuNPs surface, which allowed analyte adsorption and resulted in significant cross-reactivity. In any case, both Apt-AuNPs followed the typical response observed when aptamers are used with AuNPs, a decrease in their stability against salt-induced aggregation after target binding by the aptamer, as shown schematically in Figure 2E. It is proposed that target binding resulted in the aptamer adopting a conformation that resembled ds-DNA, minimizing the interactions between the aptamer and the AuNPs surface. As a result, the Apt-AuNPs became less stable and were more prone to salt-induced aggregation, compared to Apt-AuNPs exposed to non-target analytes or a blank.

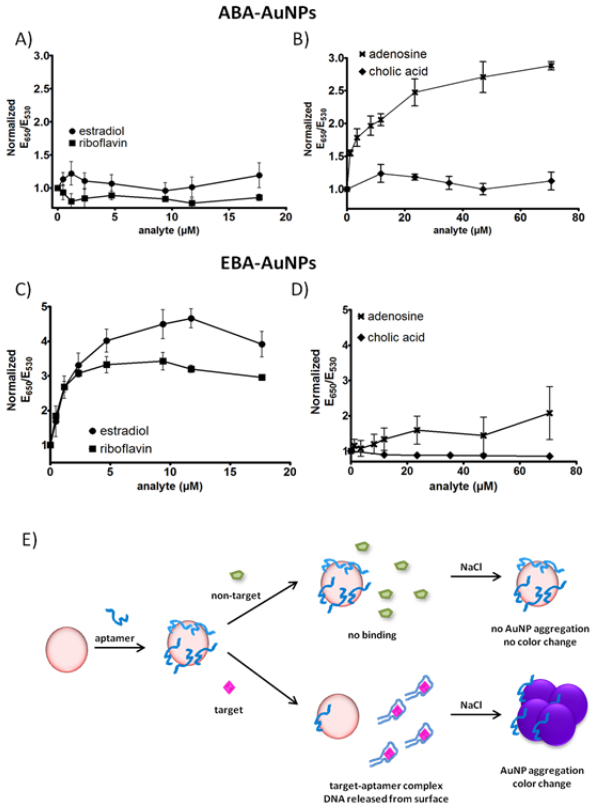

Fig. 2 Characterization of Apt-AuNPs cross-reactivity to different analytes. A) and B): ABA-AuNPs in 424 mM NaCl, data obtained two minutes after NaCl addition, C and D): EBA-AuNPs in 150 mM NaCl, data obtained two minutes after NaCl addition; data show the standard deviation of three replicates, E: proposed response mechanism.

The CABA-AuNPs did not respond to any analyte when they were tested in the same format as the ABA- and EBA-AuNPs, namely, they did not show a larger aggregation degree in the

presence of cholic acid after NaCl addition, compared to the blank. Using increasing concentrations of salt in the assay to promote severe aggregation of the CABA-AuNPs suggested that cholic acid binding by the CABA-AuNPs resulted in an increased stability of the conjugates, compared to the controls. It is important to note that the assay optimization in this case is different from the assay discussed in the previous section. The CABA-AuNPs were exposed to NaCl concentrations that promoted their aggregation in the absence of any analyte. These same conditions were used in the presence of cholic acid and the other analytes. As shown in Figure 3A and B the CABA-AuNPs responded to cholic acid, with negligible responses to all non-target molecules. It could be argued that the response observed was due to cholic acid adsorption on the AuNPs without aptamer binding, however, the fact that there was no effect observed with adenosine even at high concentrations suggested that surface passivation by aptamer adsorption was optimal and prevented non-specific interactions. Figure S4 in the supplementary information shows TEM images of CABA-AuNPs exposed to buffer (Figure S4A) and cholic acid (S4B). The images showed that the colorimetric response reported is, in fact, due prevention of AuNPs aggregation due to cholic acid binding. Interestingly, target binding-induced Apt-AuNPs stability has previously been observed with the riboflavin aptamer. We have reported the design of RBA-AuNPs that responded to riboflavin at sub-micromolar levels with no response to 2-quinoxaline carboxylic acid (QCA), the chemical used in the negative selection step during SELEX[24]. As shown in Figure S2, riboflavin adsorption on citrate-stabilized AuNPs promoted AuNPs aggregation, therefore, analyte adsorption can be ruled out as the cause of the observed increased stability after riboflavin binding. In this study, we expanded the RBA-AuNPs response characterization by exposing them to the other analytes. Figure 3C and D shows that a response to cholic acid was observed, with no responses to estradiol or adenosine, again confirming that non-specific analyte-AuNPs interactions were prevented.

Figure 1A and S1 shows that the CABA adopts a three-way junction structure, similar to the well-studied cocaine binding aptamer[42] (CoBA), while the RBA adopts the well-characterized G-quartet conformation. It is important to notice that our work shows that two aptamers with significant different structural features provided extra stability to the AuNPs upon target binding (RBA and CABA), while two aptamers with similar structures showed the opposite stabilization effect (CABA promoted increase in stability while CoBA resulted in decreased stability). These results seemed to indicate that the type of responses obtained with Apt-AuNPs cannot be predicted only by analyzing the aptamer structure. The exact reason for an aptamer to promote or prevent salt-induced aggregation in the Apt-AuNPs upon target binding is not clear yet, but we hypothesized that is a combination of complex surface-aptamer, target-aptamer, and target-surface interactions. This phenomenon is currently under investigation in our group. Importantly, this target binding-induced AuNP stability enhancement resembles what has been reported for thiol-anchored aptamers on AuNPs[43]. In this case, since the aptamers were covalently bound to the AuNPs surface, they could not be released upon target binding. It was proposed that the more compact aptamer-target complex formed on the AuNPs surface improved AuNPs stability by increasing the surface charge density near the AuNPs surface. We believe a similar mechanism is responsible for the effect observed here, as shown schematically in Figure 3E. Target binding allowed the aptamer to fold into a more compact structure that interacted strongly with the AuNPs surface, increasing the Apt-AuNPs stability against salt-induced aggregation. The data from these four Apt-AuNPs suggested that minimizing direct surface-analyte interactions was not enough to prevent responses to non-target analytes. While these responses to non-targets could be seen as a weakness of these colorimetric sensors, it has been shown that sensors that respond to multiple targets with *different* affinities can be used to create cross-reactive sensors that mimic the human nose and tongue. Based on this concept, we analyzed the data of all sensors combined per target, as shown in Figure 4, to determine if these Apt-AuNPs could be used as cross-reactive sensors, as will be discussed in the next section.

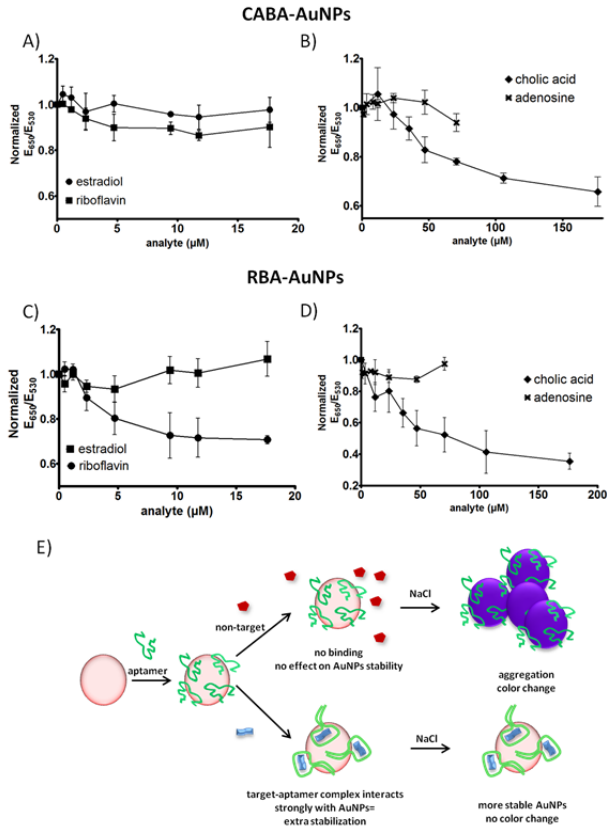

Fig. 3 Characterization of Apt-AuNPs cross-reactivity to different analytes. A) and B): CABA-AuNPs in 370 mM NaCl, data obtained two minutes after NaCl addition, C and D): RBA-AuNPs in 333 mM NaCl, data obtained two minutes after NaCl addition; data show the standard deviation of three replicates, E: proposed response mechanism.

Plasmonic Fingerprint Analysis

Cross reactive sensors try to mimic the human nose by detecting targets using a number of sensing subunits that respond with different affinities to different analytes. Ideally, when the output of each sensor subunit is combined, a unique fingerprint for each

target is obtained. Most of the literature dealing with nanomaterials-based cross reactive arrays has focused on the identification of protein or cellular targets. This is due to the large number of functional groups present in these species, which improves the possibilities of observing different responses to each analyte with a cross reactive array. Small molecules on the other hand, due to their lower number of functional groups, are more challenging analytes, which required sensors with more powerful discrimination capabilities. Aptamers, due to their complex structural features have been shown to differentiate between analytes with similar chemical structures, showing promise for small molecule fingerprint identification. Analysis of our results suggested that a qualitatively different fingerprint for each analyte studied here could be generated by combining the response of each Apt-AuNP to the same target (Figure S5). The data shows that the cholic acid and adenosine fingerprints are easy to identify (Figure S5A and B, respectively). However, the fingerprints obtained for riboflavin and estradiol looked similar at first (Figures S5C and D, respectively), due to the dominant response given by the EBA-AuNPs (green bars). Notably, the fact that two different mechanisms of response were observed, allowed to clearly identify each target, as shown in the insets in the fingerprint plots for riboflavin and estradiol.

Importantly, the analyte fingerprints allowed not only their qualitative identification but detailed analysis of the data showed that analyte quantification was possible as well. As shown in Figure 4A, a different fingerprint was obtained with each target at the different concentrations tested. For clarity of comparison, the Apt-AuNPs response to the analytes at 15 and 20 µM (five replicates) was plotted side-by-side (Figure 4A), showing that the fingerprint "shape" was analyte concentration-dependent. From the point of view of simplicity of sensor design, it is preferred to use the minimum number of sensors units that provide enough discrimination power to identify the analytes of interest. Moreover, since aptamer selection could be a time consuming process and often quite challenging to implement for small molecule targets, it would be ideal to utilize the minimum number of aptamers to detect the larger number of analytes possible. To test this idea, we compared the fingerprint generated with the original four Apt-AuNPs and three Apt-AuNPs, after removing the data from the ABA-AuNPs, which was the least cross-reactive sensor. It was clearly observed that the discrimination power of the cross-reactive sensors was maintained when only three Apt-AuNPs were used, as observed by the different fingerprints obtained at both concentrations analyzed (Figure 4B).

Visual identification and quantification of analytes fingerprint could be a tedious process. To simplify the data analysis from these cross-reactive sensors, a training set was obtained to determine whether principal components analysis (PCA) could be used to perform the analyte identification. To do this, five replicates of each data set were obtained per analyte studied at a concentration of 15 and 20 µM, resulting in a 5x4x9 matrix (five replicates, four sensors, and nine samples-one buffer and each analyte at two different concentrations-, the raw data is shown in Table S1). The Apt-AuNPs responses to the analytes studied were analyzed using PCA (see results in Table S2). Four canonical factors were obtained, with F1 (66.42%) and F2 (22.23%)

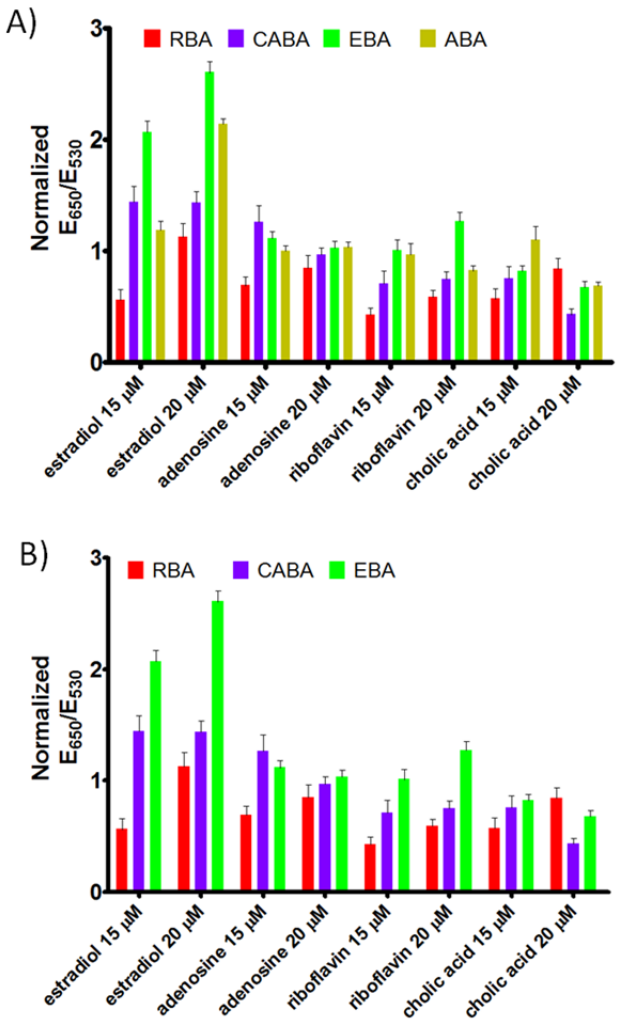

Fig. 4 Fingerprint-based analyte identification at different concentrations. Comparison of the fingerprints obtained with analytes concentrations of 15 and 20 µM using: A) Four Apt-AuNPs, and B) Three Apt-AuNPs (after removal of the ABA-AuNPs data, the least responsive of the sensors). Error bars show the standard deviation of six replicates.

accounted for most of the data variation (88.66%). Figure 5A, shows a PCA score plot using F1 and F2. Importantly, each analyte resulted in a different cluster that could be used for qualitative identification. Moreover, different concentrations of the same target resulted in different clusters, suggesting that these Apt-AuNPs could potentially be used for analyte quantification as well. The response of three Apt-AuNPs (without the ABA-AuNPs, the least cross-reactive sensor) was analyzed by PCA as well, Figure 5B. Three canonical factors were obtained with F1 (66.01%) and F2 (29.14%) accounting for most of the variability (95.16%). It was observed that the three sensor matrix offered an optimal discrimination power, showing different clusters per each analyte at each concentration tested. In fact, no loss in the data resolution was observed when reducing the sensor matrix from four to three Apt-AuNPs. As discussed in the previous section,

this data suggested that an aptamer for each analyte of interest is not necessary to create cross-reactive sensors, rather, it seems that a combination of a few aptamers with broad selectivities provide enough discrimination power for analyte sensing. Currently, we

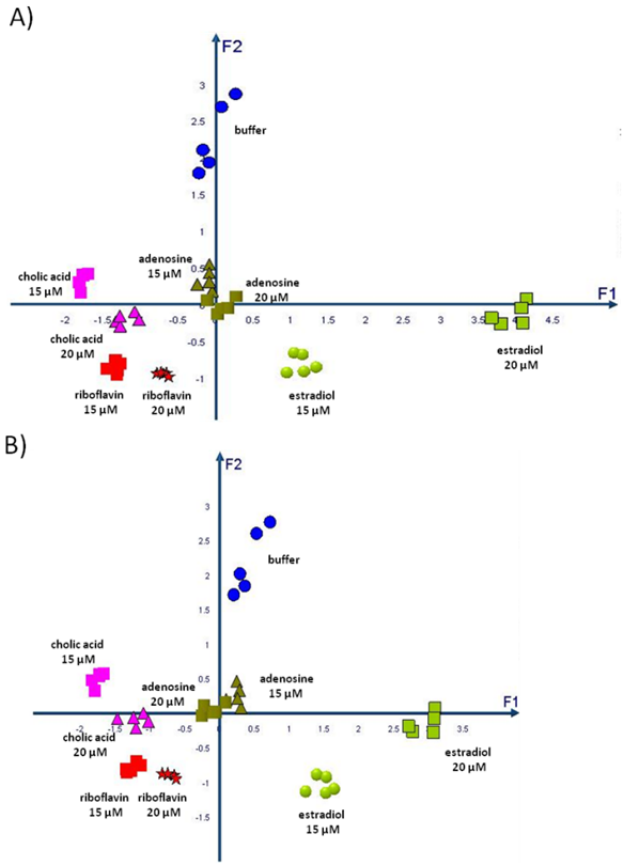

Fig. 5 Principal Components Score Plot. The Apt-AuNPs response to the analytes of interest was analyzed by PCA, the sample set contained one buffer (blank) and each analyte at two concentrations: 15 and 20 µM. Analysis of data generated by A) the four Apt-AuNPs and B) three Apt-AuNPs (without the ABA-AuNPs data).

are exploring larger analyte sets with Apt-AuNPs libraries of different sizes to identify the minimum number of Apt-AuNPs necessary to identify a fixed number of targets.

Conclusions

In this work, we designed Apt-AuNPs with aptamers that bind small molecules. Colorimetric assays for each target were optimized and tested against multiple targets to determine whether these sensors show any cross-reactivity. Importantly, during these studies two different types of responses of the Apt-AuNPs to the aptamers' target were observed. In the case of the estradiol-binding aptamer and the adenosine-binding aptamer, Apt-AuNPs showed a higher tendency to aggregate after target-binding, as was expected based on other AuNP-based assays reported in the literature. Both, the riboflavin-binding aptamer and cholic acid-binding aptamer showed the opposite response, namely, that Apt-AuNPs became more stable upon target binding. The exact reason for this difference in response is not clear yet but seems to be due to specific aptamer-AuNPs interactions, probably related to the specific aptamer sequence and changes in its conformation in the unbound and bound state. The assays response characterization showed some cross-reactivity with non-target analytes. This cross-reactive nature of these Apt-AuNPs response was utilized to demonstrate for the first time a plasmonic multiplex sensor for small molecular targets. Principal components analysis was shown to cluster the data efficiently, allowing unambiguous analyte identification and quantification. This work opens the door to utilize the plasmonic response of Apt-AuNPs to design fast cross-reactive sensors for small molecules. We envisioned that coupling these detection systems to cell-phone based assay analysis will allow the use of these sensors in point of care diagnostics applications.

Acknowledgements

This work was partially funded by the Air Force Office of Scientific Research and the Defense Forensic Science Center.

References

1. B. Duncan, S. G. Elci, V. M. Rotello, , *Nano Today,* 2012, 228-230
2. G. Poste, *Trends in Molecular Medicine,* 2012, **18**(12), 717-722
3. J. F. Rusling, *Anal. Chem*., 2013, **85**, 5304-5310
4. M. McKeague, and M. C. DeRosa, *Journal of Nucleic Acids,* 2012,Volume 2012, Article ID 748913
5. M. N. Stojanovic, and D. M. Kolpashchikov, *J. Am. Chem. Soc*., 2004, **126**, 9266-9270
6. O. R. Miranda, B. Creran, V. M. Rotello, *Current Opinion in Chemical Biology* 2010, **14**, 728-736
7. G. J. Worsley, S. L. Attree, J. E. Noble, A. M. Horgan, *Biosens. and Bioelectron*., 2012, **34**, 215-220
8. C-C. You, O.R. Miranda,B. Gider, P.S. Ghosh, I-B Kim, B. Erdogan, S. A. Krovi, U. H. F. Bunz, V. M. Rotello, *Nat. Nanotechnol*., 2007, **2**, 318-323
9. J. J. Lavigne, and E. V. Anslyn, *Angew., Chem. Int. Ed.,* 2001, **40**, 3118-3130
10. K. Saha, S. S. Agasti, C. Kim, X. Li, V. M. Rotello, *Chem. Rev.,* 2012, **112**, 2739-2779
11. K. L. Diehl, and E. V. Anslyn, *Chem. Soc. Rev.,* 2013, **42**, 8596-8611
12. N. O. Fisher, T. M. Tarasow, J.B-H. Toh, *Current Opinion in Chemical Biology* 2007, **11**, 316-328
13. M. Famulok and G. Mayer, *Accounts of Chemical Research* 2011, **44**(12), 1349-1358
14. A. B. Iliuk, L. Hu, W. A. Tao, *Anal. Chem*. 2011, **83**, 4440-4452
15. J. H. Lee, M. V. Yigit, D. Mazumdar, Y. Lu, *Advanced Drug Delivery Reviews,* 2010, **62**, 592-605
16. T. Kato, K. Yano, K. Ikebukuro, I. Karube, *Nucleic Acids Research,* 2000, **28**, 9, 1963-1968
17. M. N. Stojanovic, E. G. Green, S. Semova, D. B. Nikić, D. W. Landry, *J. Am. Chem. Soc*., 2003, **125**, 6085-6089
18. N. Derbyshire, S. J. White, D. H. J. Bunka, L. Song, S. Stead, J. Tarbin, M. Sharman, D. Zhou, P. G. Stockley, *Anal. Chem.*, 2012, **84**, 6595-6602
19. C. Rosman, J. Prasad, A. Neiser, A. Henkel, J. Edgar, C. Sönnichsen, *Nano Lett.,* 2013, **13**, 3243-3247
20. G. Wang, Y. Wang, L. Chen, J. Choo, *Biosens Bioelectron*. 2010, **25**, 1859-1868
21. F. Xia, X. Zuob, R. Yang, Y. Xiao, D. Kang, A. Vallée-Bélisle, X. Gong, J. D. Yuen, B. B. Y. Hsu, A. J. Heeger, K. W. Plaxco, *Proc. Natl. Acad. Sci U.S.A.*, 2010, **107**(24), 10837-10841
22. L. Wang, X. Liu, S. Song, C. Fan, *Chem. Commun*., 2006, 3780-3782
23. J. L. Chávez, W. Lyon, N. Kelley-Loughnane, M. O. Stone, *Biosens. Bioelectron*., 2010, **26**, 23-28

24. J. L. Chávez , R. I. MacCuspie, M. O. Stone, N. Kelley-Loughnane, *J. Nanopart. Res.,* 2012, **14**:1166
25. J. Liu, Y. Lu, *Angew Chem Int Ed,* 2006, **45**, 90-94
26. V. Pavlov, Y. Xiao, B. Shlyahovsky, I. Willner, , *J Am Chem Soc,* 2004,**126**, 11768-11769
27. H. Li, L. Rothberg, *Proc Natl Acad Sci USA,* 2004, **101**, 14036-14039
28. J. Zhang, L. Wang, D. Pan, S. Song, F. Y. C. Boey, H. Zhang, C. Fan, *Small* 2008, **8**, 1196-1200
29. J. E. Smith, D. K. Griffin, J. K. Leny, J. A. Hagen, J. L. Chávez, N. Kelley-Loughnane, *Talanta,* 2014, **121**, 247-255
30. U. H. F. Bunz, V.M. Rotello, *Angew. Chem. Int. Ed.,* 2010, **49**, 3268 – 3279
31. X. Li, F. Wen, B. Creran, Y. Jeong, X. Zhang, V. M. Rotello, *Small,* 2012, **8**, 3589-3592
32. Y. Lu, Y. Liu, S. Zhang, S. Wang, S. Zhang, X. Zhang, *Anal. Chem*., 2013, **85**, 6571-6574
33. C. Zhang, L. Wang, Z. Tu, X. Sun, Q. He, Z. Lei, C. Xu, Y. Liu, X. Zhang, J. Yang, X. Liu, Y. Xu, *Biosens. Bioelectron.,* 2014, **55**, 216-219
34. S. Pang, T. P. Labuzab, L. He, *Analyst,* 2014, **139**, 1895-1901
35. D. E. Huizenga, J. W. Szostak, *Biochemistry,* 1995, **34**, 656-665
36. C. T. Lauhon, J. W. Szostak, *J. Am. Chem. Soc.*, 1995, **117**, 1246-1257
37. Y. S. Kim, H. S. Jung, T. Matsuura, H-Y Lee, T. Kawai, M. B. Gu, Biosens. Bioelectron., 2007, **22**, 2525-2531
38. T. Kato, T. Takemura, K. Yano, K. Ikebukuro, I. Karube, *Biochimica et Biophysica Acta* 2000, **1493**, 12-18
39. M. Zheng, F. Davidson, X. Huang, *J. Am. Chem. Soc*., 2003, **125**, 7790-7791
40. S. H De Paoli Lacerda, J. J. Park, C. Meuse, D. Pristinski, M. L. Becker, A. Karim, J. F. Douglas, *ACS Nano,* 2010, **4**(1), 365-379
41. C. H. Lin, D. J. Patel, *Chemistry & Biology,* 1997, **4**(11), 817-832
42. M. A. D. Neves, O. Reinstein, P.E. Johnson, *Biochemistry,* 2010, **49**, 8478-8487
43. W. Zhao, W. Chiuman, J. C. F. Lam, S. A. McManus, W. Chen, Y. Cui, R. Pelton, M. A. Brook, Y. Li, *J Am Chem Soc,* 2008, **130**, 3610–3618

Notes and References

[a] *Human Effectiveness Directorate, 711th Human Performance Wing, Air Force Research Laboratory, Wright-Patterson Air Force Base, OH 45433, United States,. Fax: XX XXXX XXXX; Tel: XX XXXX XXXX; E-mail: xxxx@aaa.bbb.ccc*
[b] *Current address: College of Engineering and Applied Science, School of Electronic and Computing Systems, University of Cincinnati, 812 Rhodes Hall, Cincinnati, OH 45221, United States*
[c] *Current address: College of Arts and Sciences, Department of Chemistry and Biochemistry, Ohio State University, 1110 Newman and Wolfrom Laboratory, Columbus, OH 43210, United States*
† Electronic Supplementary Information (ESI) available: mfold-predicted aptamer structures, AuNPs aggregation in the presence of analytes, TEM images of Apt-AuNPs after NaCl addition in the presence and absence of DNA, raw data used to performed PCA analysis and principal components values obtained. See DOI: 10.1039/b000000x/
‡ Footnotes should appear here. These might include comments relevant to but not central to the matter under discussion, limited experimental and spectral data, and crystallographic data.

Appendix: Supplemental Figures

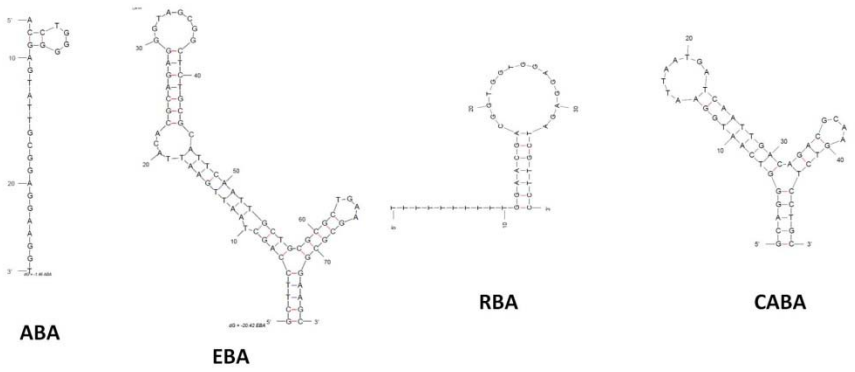

Figure S1. Mfold Predicted Structures of DNA Aptamers used in this Study

Notice that mfold did not predict the experimentally observed structures for ABA (pseudohelix) and RBA (G-quartet). Structures were folded at 25 °C, 5 mM NaCl, 1 mM $MgCl_2$, to mimic our experimental conditions.

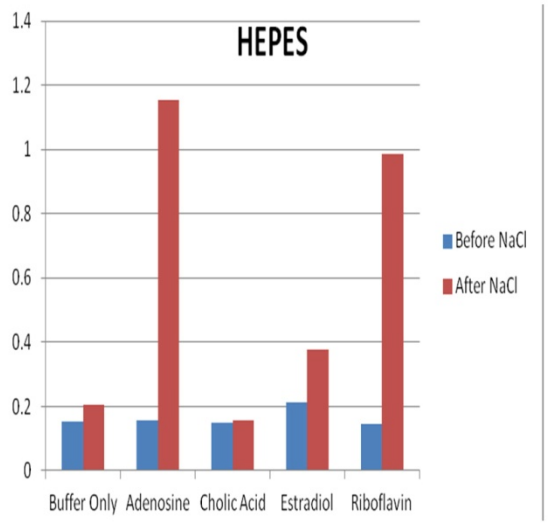

Figure S2. Citrate-Stabilized AuNPs Aggregation in the Presence of Different Analytes.

AuNPs were suspended in 10 mM HEPES, 1 mM $MgCl_2$, pH 7.4 (HEPES buffer). AuNPs aggregation degree before (blue bars) and after (red bars) NaCl addition a mixture of 90 µL AuNPs in HEPES buffer and 10 µL of 180 µM different analytes dissolved in HEPES buffer.

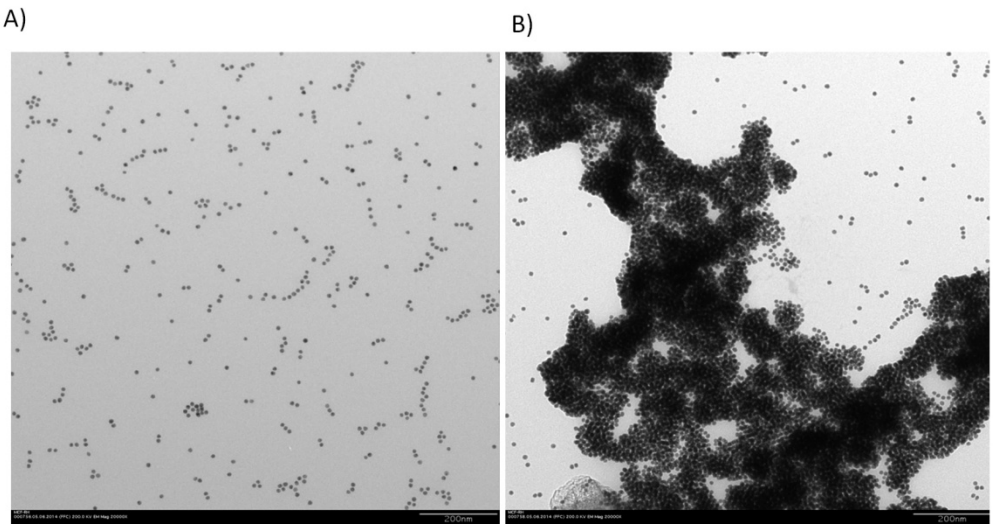

Figure S3: TEM Images of ABA-AuNPs

Images showed the aggregation of ABA-AuNPs exposed to A): buffer and B) adenosine (20 µM), after addition of NaCl

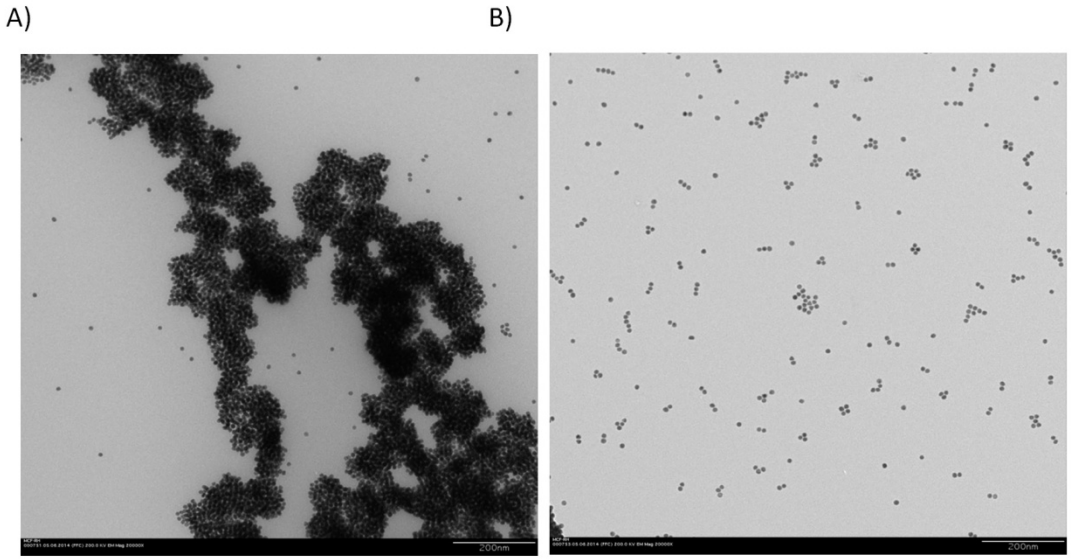

Figure S4: TEM Images of CABA-AuNPs

Images showed the aggregation of CABA-AuNPs exposed to A): buffer and B) cholic acid (50 µM), after addition of NaCl

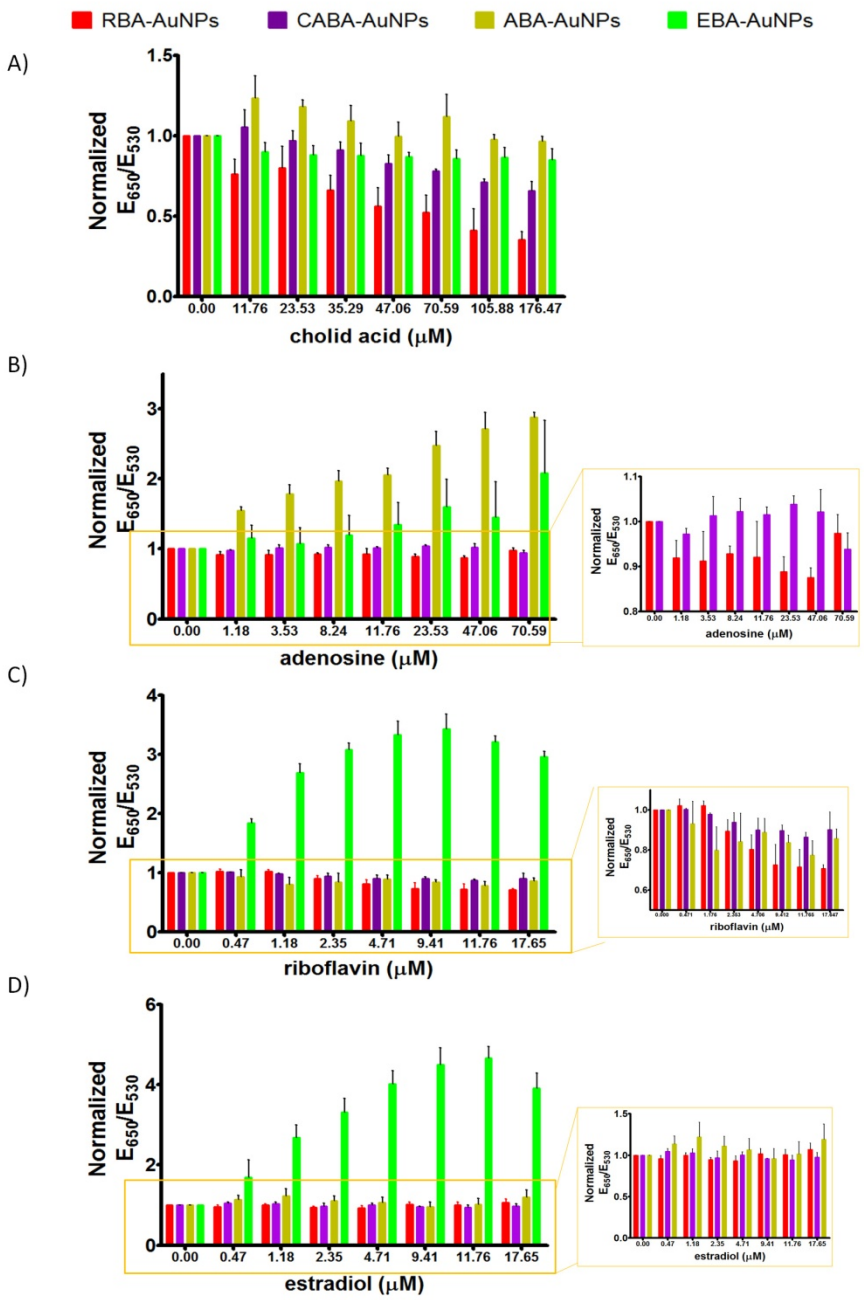

Figure S5: Fingerprint Data Analysis

The responses from the four Apt-AuNPs designed in this work were combined to obtain a fingerprint per analyte studied. Insets show the "stabilization effect" that allowed a more efficient analyte differentiation.

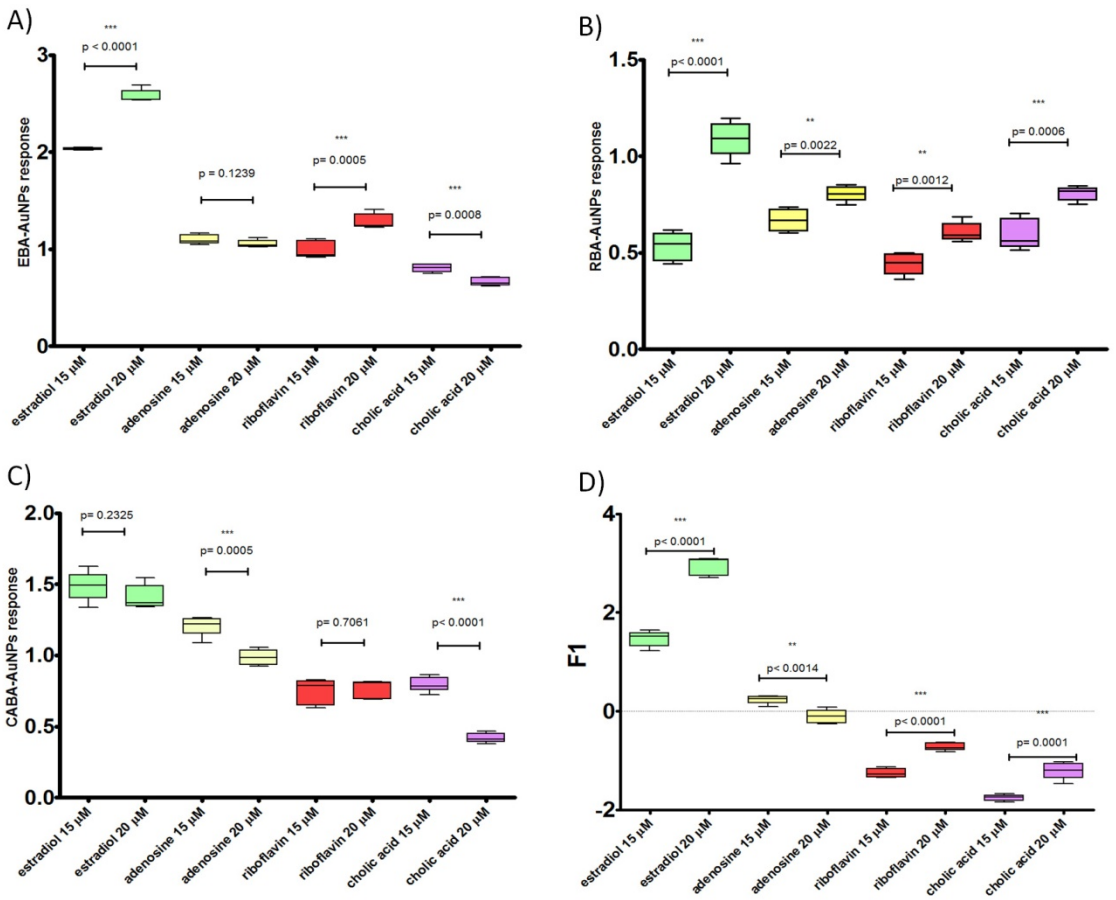

Figure S6: T-Test Analysis

The Apt- AuNPs response was further analyzed to determine the statistical differences of the output obtained with the analytes at different concentrations. The results are presented in Figure S6. Each plot shows the results of one Apt-AuNP exposed to each analyte at two different concentrations. These two values were analyzed using the t-test. It was observed that, in most cases, a statistically different response was obtained. Analysis of the output per Apt-AuNPs has limited practical relevance since it was established in this work that the combined response of the sensors provides a superior means for analyte identification and quantification. Therefore the PCA output was analyzed in a similar manner, comparing the first principal component of each sensor. Figure S6 D shows that in all cases the responses observed with different concentrations of the same target were significantly different, confirming the superior analytical performance when the Apt-AuNPs were used as cross-reactive sensors.

Table S1: Apt-AuNP Size Analysis by Dynamic Light Scattering

CABA-AuNPs	peak 1			peak 2				
	size	**%**	**SD**	**size**	**%**	**SD**	**Zav**	**PDI**
blank no salt	15.76	93	5.95	368	6.8	120	16.74	0.191
blank + 300 mM NaCl	251.7	87.1	66.72	82.59	12.9	125.5	181	0.244
50 uM CA+ 300 mM NaCl	101.8	73.11	61.6	16.98	26.9	13.31	47.69	0.512

EBA-AuNPs	peak 1			peak 2			peak 3				
	size	**%**	**SD**	**size**	**%**	**SD**	**size**	**%**	**SD**	**Zav**	**PDI**
blank no salt	18.63	94.1	6.02	4.94	2.6	0.54	4152	3.3	1024	16.75	0.192
blank + 172 mM NaCl	88.66	50.3	28.27	16.57	41.3	3.24	1490	8.4	612.5	32.84	0.479
5 uM Est+ 172 mM NaCl	87.97	77.5	21.19	17.75	22.5	2.172				50.94	0.444

Apt-AuNPs were prepared as described in the experimental section. Samples were analyzed in a Zetasizer Nano Istrument (Malvern Instruments, Westborough, MA) utilized in backscatter mode (173 detection angle) with the temperature set at 20.0 °C. Apt-AuNPs (75 µL) were mixed with 10 µL of assay buffer (blank) or the analyte of interest in assay buffer and incubated for one minute. This was followed by NaCl addition (exact concentrations are listed on Table S1), and after another one-minute incubation, the size was determined by DLS.

Table S2: Data Utilized for PCA Analysis

	ABA	EBA	RBA	CABA
buffer 1	0.265957	0.239474	0.275401	0.501433
buffer 2	0.270053	0.248	0.268617	0.52149
buffer 3	0.281501	0.257979	0.308108	0.480114
buffer 4	0.284211	0.255937	0.272727	0.52071
buffer 5	0.265416	0.248021	0.259259	0.530259
estradiol 1	0.579387	0.667638	0.298343	0.74772
estradiol 2	0.574586	0.663768	0.312668	0.737805
estradiol 3	0.589385	0.649718	0.321716	0.742424
estradiol 4	0.555241	0.637883	0.296	0.697605
estradiol 5	0.571429	0.628571	0.290667	0.725076
adenosine 1	0.289817	0.267532	0.241558	0.511364
adenosine 2	0.299479	0.260982	0.221932	0.461957
adenosine 3	0.291777	0.264935	0.228792	0.495798
adenosine 4	0.263708	0.239401	0.23057	0.480226
adenosine 5	0.278947	0.253071	0.226221	0.5
riboflavin 1	0.219321	0.315508	0.155844	0.404372
riboflavin 2	0.220472	0.307278	0.158442	0.382514
riboflavin 3	0.218182	0.320955	0.159794	0.389503
riboflavin 4	0.223377	0.31383	0.158031	0.359673
riboflavin 5	0.227513	0.324397	0.159269	0.365854
cholic acid 1	0.186667	0.176966	0.232	0.2
cholic acid 2	0.189474	0.160105	0.233244	0.228495
cholic acid 3	0.187831	0.16	0.213542	0.223404
cholic acid 4	0.18617	0.163102	0.231608	0.213333
cholic acid 5	0.195187	0.16129	0.224	0.2

Table S3: Results of PCA Analysis of the Data of the Four Sensors

(data shown in Table S1)

Observation	F1	F2	F3	F4
buffer 1	0.262	2.867	-0.323	-0.071
buffer 2	0.074	2.691	-0.363	-0.252
buffer 3	-0.228	1.789	-0.359	-0.039
buffer 4	-0.091	1.933	-0.419	-0.059
buffer 5	-0.172	2.103	-0.412	-0.160
15estradiol 1	0.945	-0.928	-1.196	-0.231
15estradiol 2	1.152	-0.682	-1.299	-0.007
15estradiol 3	1.173	-0.914	-1.244	0.165
15estradiol 4	1.334	-0.855	-1.277	-0.047
15estradiol 5	1.043	-0.659	-1.331	-0.353
20estradiol 1	4.087	-0.252	0.610	-0.204
20estradiol 2	4.066	-0.047	0.583	-0.257
20estradiol 3	4.137	0.078	0.722	-0.244
20estradiol 4	3.670	-0.183	0.605	-0.310
20estradiol 5	3.800	-0.267	0.737	-0.169
15adenosine 1	-0.089	0.306	-0.497	0.253
15adenosine 2	-0.088	0.428	-0.450	0.432
15adenosine 3	-0.248	0.271	-0.341	0.536
15adenosine 4	-0.050	0.182	-0.424	0.624
15adenosine 5	-0.087	0.544	-0.379	0.326
20adenosine 1	0.263	0.107	0.542	0.659
20adenosine 2	0.018	-0.128	0.683	0.423
20adenosine 3	0.155	-0.051	0.589	0.601
20adenosine 4	-0.114	0.053	0.517	0.670
20adenosine 5	0.063	-0.053	0.554	0.700
15riboflavin 1	-1.312	-0.905	-0.083	-0.551
15riboflavin 2	-1.447	-0.875	-0.141	-0.510
15riboflavin 3	-1.340	-0.753	-0.052	-0.020
15riboflavin 4	-1.320	-0.956	0.133	-0.270
15riboflavin 5	-1.275	-0.807	-0.109	-0.094
20riboflavin 1	-0.631	-0.980	0.058	0.278
20riboflavin 2	-0.730	-0.923	0.108	0.179
20riboflavin 3	-0.661	-0.930	0.033	0.178
20riboflavin 4	-0.786	-0.933	0.115	0.030
20riboflavin 5	-0.702	-0.942	0.095	0.016
15cholic acid 1	-1.775	0.389	0.434	-0.428
15cholic acid 2	-1.703	0.418	0.501	-0.233

15cholic acid 3	-1.804	0.163	0.517	-0.221
15cholic acid 4	-1.773	0.402	0.479	-0.312
15cholic acid 5	-1.819	0.301	0.561	-0.388
20cholic acid 1	-1.282	-0.158	0.247	-0.100
20cholic acid 2	-1.023	-0.211	0.288	0.018
20cholic acid 3	-1.274	-0.298	0.188	-0.008
20cholic acid 4	-1.336	-0.237	0.497	-0.402
20cholic acid 5	-1.081	-0.102	0.300	-0.149

Table S4: Results of PCA Analysis of the Data of the Three Sensors

(without sensor ABA-AuNPs, data shown in Table S1).

	F1	F2	F3
buffer 1	0.581	19.388	0.788
buffer 2	0.312	17.148	2.579
buffer 3	0.044	7.433	0.631
buffer 4	0.143	8.592	0.907
buffer 5	0.093	10.313	1.755
15estradiol 1	1.697	3.276	5.957
15estradiol 2	2.612	2.189	3.165
15estradiol 3	2.589	3.400	1.119
15estradiol 4	3.018	3.069	3.485
15estradiol 5	2.170	2.013	9.554
20estradiol 1	10.564	0.199	0.237
20estradiol 2	10.640	0.016	0.059
20estradiol 3	10.700	0.011	0.237
20estradiol 4	8.234	0.094	0.003
20estradiol 5	8.601	0.178	0.605
15adenosine 1	0.073	0.111	0.029
15adenosine 2	0.088	0.273	0.774
15adenosine 3	0.009	0.094	2.000
15adenosine 4	0.103	0.016	2.668
15adenosine 5	0.065	0.537	0.348
20adenosine 1	0.008	0.061	10.202
20adenosine 2	0.077	0.003	6.445
20adenosine 3	0.004	0.000	9.319
20adenosine 4	0.056	0.031	10.050
20adenosine 5	0.011	0.000	11.237
15riboflavin 1	1.821	1.756	4.704
15riboflavin 2	2.039	1.664	4.465
15riboflavin 3	1.610	1.251	0.043
15riboflavin 4	2.022	1.875	0.692
15riboflavin 5	1.444	1.478	0.301
20riboflavin 1	0.444	2.276	1.223
20riboflavin 2	0.629	1.939	0.654
20riboflavin 3	0.481	2.035	0.491
20riboflavin 4	0.768	1.934	0.074
20riboflavin 5	0.631	2.000	0.040
15cholic acid 1	3.387	0.736	1.184
15cholic acid 2	3.134	0.816	0.078
15cholic acid 3	3.607	0.262	0.042

15cholic acid 4	3.380	0.777	0.362
15cholic acid 5	3.804	0.569	0.574
20cholic acid 1	1.720	0.010	0.009
20cholic acid 2	1.181	0.039	0.173
20cholic acid 3	1.622	0.120	0.025
20cholic acid 4	2.431	0.018	0.681
20cholic acid 5	1.351	0.000	0.034